coatings

Article

Functional Olive Pit Powders: The Role of the Bio-Based Filler in Reducing the Water Uptake Phenomena of the Waterborne Paint

Massimo Calovi * and Stefano Rossi

Department of Industrial Engineering, University of Trento, 38123 Trento, Italy
* Correspondence: massimo.calovi@unitn.it; Tel.: +39-0461-282442

Abstract: In this study, olive pit powders were added to a polyurethane-acrylate paint for examining the impact of two alternative functionalization processes in increasing the filler hydrophobicity in an effort to increase the durability of the paint. In order to look into potential changes in morphology and appearance owing to the surface conversion treatments of the two bio-based additives, the coatings were examined using electron microscopy and colorimetric tests. The coating's resilience and the hydrophobic/hydrophilic role of the fillers were evaluated by salt spray chamber exposure, contact angle measurements, paint liquid resistance, UV-B exposure, and electrochemical impedance spectroscopy measurements, which highlighted the reduction in water absorption inclination of the filler made of lignocellulose due to the silane and wax functionalization. This study demonstrated that the bio-based filler, if properly functionalized, can actually be implemented as multifunctional pigment in waterborne paints, giving specific aesthetic characteristics, but also improving the barrier performance of the polymeric matrix and increasing the durability of the composite coating.

Keywords: bio-based filler; olive pit waste; ecofriendly paint; natural pigment; paint durability

1. Introduction

The prices of raw materials have continuously increased during the last century, due to an unsustainable linear economy. Because to this process, resources are becoming more precious, the environment is being irreparably scarred, and waste is amassing [1]. As a counteroffensive to this phenomenon, a new type of economy, defined as 'regenerative', is developing. This strategy focuses mostly on elements like the circular production/consumption system with the intention of minimizing the impact on the environment [2]. In this scenario, sustainable sources, such as bio-based materials, are applied to replace the petroleum-based products, in order to optimize the waste management systems. For example, the application of purely natural fillers or deriving from industrial trash is attracting great interest in the field of composite materials and coatings [3,4]. In fact, the entire business district is constantly looking for sustainable and multifunctional replacements to the standard artificial additives [5,6], which, historically, do not consider aspects such as environmental sustainability [7].

Nowadays, food and natural waste represent important resources for the creation of fillers, which, in addition to giving fresh identity to the recycled material, add value to the composite product and reduce its production costs [8]. For instance, a study estimated that the percentage of bio-based feedstock used in the manufacturing of products will rise from 5% in 2004 to 12% in 2010, and then to about 18% in 2020. In 2030, the same study predicts a further 25% growth in use [9]. This phenomenon is supported by the international industry of agriculture and food manufacturing, which produces around 140 billion tons of biomass leftovers annually: these scraps might be a source of inexpensive, plentiful, and renewable resources [10,11].

Considering these aspects, the industrial sector is increasingly turning to the application of bio-based additives in polymeric materials with natural sources or generated from agricultural and food refuse [12]. The chicken eggshells (ES), for example, representing the greatest calcium carbonate natural resources (95%) to find in bio-waste condition [13], are widely employed as bio-filler in polypropylene hybrid material [14], acrylic coating [15], chitosan nanocomposite [16], and intumescent coatings [17,18] as a substitute to the standard industrial calcium carbonate. Similarly, the debris from various mollusks' seashells is an endless supply of $CaCO_3$, which may be employed to enhance the mechanical [19,20] and thermal [21] properties of bio-composites as well as the performance of the coating in terms of smoke suppression and flame retardancy [22,23]. Finally, the enormous amount of waste generated by the agro-industrial field can be applied as a cost-effective and valuable filler. For example, almond shell [24], pistachio nutshell [11], apricot, argan shell [25], cherry seeds [26], peanut shell [27], avocado seed [28], rice husk, groundnut shell, and coconut shell [29] powders have been studied and employed as fillers for the improvement of the physical and thermal characteristics of polymer matrix composites.

However, the olive is possibly the most attractive bio-filler resource out of all food processed by-products. Despite the high-tech industrialized processes [30], the olives; production and processing field generates a relevant amount of biomass by-product, with consequent critical challenges with handling and processing. Nevertheless, the current eco-friendly regulations enforced on the olive oil industry [31], in synergy with a more sensitive culture, are concretely enhancing the waste of the olive oil business district, both economically and considering environmental protection.

The olive stone is made of a complex structure of microfibrils, which are made up of three different chemical substances, including cellulose, hemicellulose, and lignin [32]. It stands for the most significant leftover from the production of olive oil. Consequently, olive stone derivatives have also been employed as fillers in polymers, such as thermoplastics [33,34] and thermosets [35–37], with the aim of reducing the environmental impacts of the bio-based component [38]. The introduction of olive stone into the polymer results in a rise of the elastic modulus of the composite material, with the outcome of reduced tensile strength and elongation at break [39,40]. Moreover, the granules decrease the polymer impact strength, as they function as stress concentrators in the matrix [41], but the bio-based filler is able to improve the wear abrasion resistance and the stiffness of the polymer composite [42]. Thus, these characteristics make the olive pit powders an interesting contender for a suitable filler in polymeric composite materials, with great promise in a variety of industrial demands.

Despite the aforementioned interesting olive pit features, however, this bio-based material has never been considered as a filler in organic coatings and paints. Nevertheless, a recent study has highlighted the outcomes of applying various concentrations of untreated olive pit powder in a waterborne paint [43]. The research showed that the bio-based filler can serve as a versatile pigment, which can enhance the mechanical properties of the polymeric matrix, such as abrasion resistance, hardness, and static coefficient of friction, while also supplying specific aesthetic appeal. Otherwise, accelerated degradation tests, such as salt spray chamber and UV-B exposures, proved the lignocellulose-based filler's propensity to absorb water and its severe chemical-physical deterioration. In fact, the olive pit granules provoked several undesired water uptake phenomena, which happened as a result of the lignocellulose material's inherent qualities of high hydrophilicity [41,44,45].

Obviously, these negative occurrences have resulted in a significant reduction in the protective properties of the paint. Consequently, the novelty and the objective of this research are the assessment of the impact of two different surface conversion treatments of the olive pit powders in order to increase their hydrophobicity and ensure the barrier performance of the waterborne paint. The study is aimed at revealing whether specific surface conversion processes of olive pit granules are able to guarantee their application as protective fillers in organic coatings. The granules were extracted from the olive pit and functionalized with silane and wax by the manufacturer, BioPowder [46]. Silane and

wax were used as coupling agents in the surface conversion process as they are renowned in the literature for their excellent hydrophobic properties [47–50]. The coatings were spray-deposited and characterized, comparing the behavior of the two functionalized powders with that of the untreated granules. Scanning electron microscope (SEM) and colorimetric analysis were used to examine the morphological and aesthetic characteristics of the samples, respectively, to determine the effect of the surface conversion treatment of the olive pit additives. Finally, several accelerated degradation tests and electrochemical analyses ware employed to assess the result of the functionalization of the bio-based fillers on coatings durability, highlighting the hydrophilic/hydrophobic role of the olive pit powders.

2. Materials and Methods

2.1. Materials

The untreated olive pit powders and the granules functionalized with silane and wax were furnished by BioPowder (Birkirkara, Malta). Acetone was acquired from Sigma-Aldrich (St. Louis, MO, USA) and utilized. The carbon steel substrate (Q-panel type R (0.15 wt.% C-Fe bal.)—40 mm × 70 mm × 2 mm dimensions) was bought by Q-lab (Westlake, OH, USA). The waterborne 2K acrylic-based white primer paint ECOFILLER EQW and the waterborne 2K polyurethane-acrylate transparent top-coat paint IDROPUR ZW 01 were supplied by EP Vernici (Solarolo, Italy). Sodium chloride (≥99.0%) and ethanol (99.8%) were purchased from Sigma-Aldrich (St. Louis, MO, USA) and used as received. The commercial detergent disinfectant product Suma Bac D10 Cleaner and Sanitiser (Diversey Inc., Fort Mill, SC, USA) containing benzalkonium chloride (3.0–10.0 wt.%) and the cataphoretic red ink Catafor 502XC (Arsonsisi, Milan, Italy) were purchased and used for the liquid resistance tests.

2.2. Coatings Deposition

The carbon steel frames had a pre-treatment to enhance paint adhesion, employing an ultrasound degrease process with acetone for two minutes, followed by a mechanical pickling step carried out with a sandblasting treatment involving corundum powder (0.2 mm diameter—70 mesh). The process introduced a roughness (Ra) equal to 3.21 ± 0.14 μm in the steel substrates. In order to get rid of any remaining corundum particles and other contamination, a further acetone degreasing step was used.

Four sample series were produced, as summarized in Table 1.

Table 1. Labelling of samples with various olive pit powder fillers.

Sample Nomenclature	Olive Pit Powder (2 wt.%) in the Top Coat
T	/
O	untreated
S	functionalized with silane
W	functionalized with wax

First, a coating of white acrylic-based primer with a thickness of around 100 μm was applied using a spray technique. This layer was then dried for 30 min in an oven at 60 °C. The top-coat paint was therefore sprayed on and heated for 60 min at 60 °C to cure. A thickness of roughly 200 μm was observed in the ultimate coatings (primer + top coat). The four-sample series differ in the formulation of the top coat: while sample T was realized with the unmodified commercial product, samples O, S, and W were deposited by introducing a 2 wt.% of olive pit-based filler into the polyurethane matrix. The concentration of 2 wt.% was chosen, as it was demonstrated in a previous work [43] to be able to provide multifunctionality to the paint, without introducing significant defects. The three different formulations were realized by mixing the polyurethane matrix with its catalyst and the olive pit powders: To ensure the olive pit granules were evenly distributed throughout the solutions, an ultrasonic probe was used to stir the mixtures for 30 min.

Sample O contained the pure untreated olive pit powders and was used as a reference for the other samples to highlight the importance of the powder functionalization process. In contrast, sample S and sample W contain silane- and wax-functionalized powders, respectively. The three typologies of fillers were obtained from byproducts of olive oil extraction. The olive pit chunks were first mechanically removed from the pulp and shell remains. Thus, the powders were physically washed, left to dry, and filtered according to the size of their granules. Finally, the surface conversion treatments of the fillers with silane and wax were carried out by the olive pit powders manufacturer, BioPowder [51]. Unfortunately, the functionalization process carried out by the company is under industrial secrecy, so no further information can be provided on the type of silane and wax used in the surface conversion treatments of the olive pit powders.

2.3. Characterization

The structure of the granules of the three types of fillers and the layers' cross-sections were examined with the low-vacuum scanning electron microscope (SEM) JEOL IT 300 (JEOL, Akishima, Tokyo, Japan), to evaluate the compatibility of the polymeric matrix with the bio-filler. Using ImageJ software, the SEM pictures were examined to determine the size distribution of the powders. The appearance of the samples was investigated with the optical stereomicroscope Nikon SMZ25 (Nikon Instruments, Amstelveen, The Netherlands) and with a Konica Minolta CM2600d spectrophotometer (Konica Minolta, Chiyoda, Tokyo, Japan), using a D65/10° illuminant/observer configuration in SCI mode, evaluating the coloring contribution of the bio-based filler.

The effect of the olive pit functionalization on paint durability was investigated by means of different accelerated degradation tests. The samples were exposed in a salt spray chamber (Ascott Analytical Equipment Limited, Tamworth, UK) for 500 h, following the ASTM B117-11 standard [52] (5 wt.% sodium chloride solution), to assess the influence of the bio-based filler on the corrosion protection performance of the coatings in a particular aggressive environment. A mechanical scratch was realized on the surface of the painted samples to evaluate the adhesion of the coatings and analyze the role of the functionalized filler in affecting possible water uptake phenomena.

In order to evaluate the effect of the filler on the surface wettability of the coatings, contact angle measurements were performed following the ASTM D7334/08 [53] standard. A Nikon 60 mm lens f/2.8 for macro pictures was used, and the wetting angle was measured by using the NIS-Elements Microscope Imaging software (Windows Version). The drops were formed with a syringe and dropped from a height of about 2 cm. Once the drop was focused the picture was captured, the wetting angle was measured by means of the imaging software. In total, 10 measurements were performed for each sample to obtain statistical validity.

Moreover, the influence of the powders on the barrier properties of the top coat was explored with the chemical resistance tests, according to the GB/T 1733-93 standard [54]. A filter paper was dipped in 15.0% sodium chloride solution, 70.0% medical ethanol, detergent (50.0 wt.% Suma Bac D10), and red ink, respectively, to evaluate the coatings' behavior. Thus, the filter paper was placed on the surface of the coatings and covered with a glass cover. After 24 h, the glass cover and filter paper were removed, and the residual liquid on the coating surface was absorbed. The imprint and discoloration were evaluated with the colorimetric analyses. The test was carried out on five samples per series.

Otherwise, the coatings were subjected to UV-B light employing an UV173 Box Co.Fo.Me.Gra (Co.Fo.Me.Gra, Milan, Italy), following the ASTM D4587-11 (2019) standard [55]. The experiment was conducted by combining cycles of 4 h each of exposure to UV-B radiation (313 nm–60 °C) and condensed vapor (50 °C), for a total of 200 h. The deterioration of the samples was investigated by FTIR infrared spectroscopy measurements (in attenuated total reflection ATR mode) and colorimetric analyses, monitoring the samples after 24, 48, 100, and 200 h of exposure to UV-B light. The FTIR spectra were acquired with

a Varian 4100 FTIR Excalibur spectrometer (Varian Inc., Santa Clara, CA, USA), to assess the chemical modifications of the polymeric matrix.

Finally, the protective features of the composite coatings were studied by means of Electrochemical Impedance Spectroscopy (EIS) measurements, carried out with a potentiostat Parstat 2273 (Princeton Applied Research by AMETEK, Oak Ridge, TN, USA) with the software PowerSuit ZSimpWin (version 2.40) and applying a signal of about 15 mV (peak-to-peak) amplitude in the 105-10-2 Hz frequency range. The cell setup was composed of an Ag/AgCl reference electrode (+207 mV SHE) and a platinum counter electrode, immersed in the 3.5 wt.% sodium chloride solution. The samples were kept immersed in the test solution for a total of 500 h, with a testing area equal to 6.5 cm^2. The measurements were carried out on five samples per series.

3. Results and Discussion

3.1. Powders and Coatings Morphology and Aesthetic Features

Figure 1 reveals the morphology and size distribution of the three different powders involved in this study. The three images, acquired by SEM, highlight an irregular structure of the powders, which is typical of olive pit derivatives [36,43,56–58]. Energy-dispersive X-ray spectroscopy (EDXS, Bruker, Billerica, MA, USA) analysis carried out on the untreated powder demonstrated its lignocellulose nature, as it is mostly made up of carbon and oxygen (67.8 wt.% and 30.2 wt.%, respectively), in conformity with the literature [36]. Typically, the lignocellulose biomass can be considered as comprised of lignin (20 wt.%), hemicelluloses (25 wt.%), and cellulose (around 40 wt.%). Furthermore, it typically contains additional elements like moisture (≈10 wt.%), minerals (≈1 wt.%), and proteins. [38,59]. The powders treated with wax showed a very similar elemental composition, as wax can be considered as a mixture of esters, alcohols, and saturated acids. Otherwise, the analyses carried out on the powder functionalized with silane showed traces of silicon (0.5 wt.%) representative of the silane itself.

The functionalization process did not cause a significant modification of the morphology of the powders, which all appeared similar. The graphs in Figure 1 represent the size distribution of the granules of the three types of powders, realized by using ImageJ to examine the SEM pictures. The distribution of the three graphs, as well as the D10, D50, and D90 percentile values, are very similar. The average size of the powders resides at approximately 11 μm, while almost all of the granules do not exceed 55 μm. Thus, the surface conversion treatment carried out with silane or wax does not alter the structural morphology of the olive pit powder, nor does it influence the size of the granules. However, although the two surface conversion processes with silane and wax did not cause an evident morphological and structural change in the powders, the three types of fillers showed a different protective behavior, as will be described later.

Thus, the three series of powders were employed for the deposition of the coatings summarized in Table 1. The samples underwent a brittle fracture process in liquid nitrogen to observe the layer cross-section via SEM analysis. The investigation was carried out to analyze the interaction of the bio-based fillers with the paint matrix. Figure 2 represents the cross-section of sample S (containing the powder functionalized with silane): the image clearly shows the two layers constituting the coating, such as the primer and the top coat. The two films have similar thickness, of about 100 μm, and appear compact, homogeneous, and free of bubbles, which represent frequent imperfections of the layers deposited with the spray technique [60]. The presence of the filler in the top coat can be appreciated by a single granule of powder, still well anchored in the layer even after being subjected to a brittle fracture procedure. This phenomenon, observed in all three samples containing the bio-based filler, is representative of a favorable interaction between the olive pit powders and the polymeric matrix of the top coat. The literature describes some problems of compatibility of olive pit powders with polymeric matrices: drawback phenomena of the granules can lead to the development of phase boundary and cavity

gaps [57,58]. However, the three series of powders employed in this work evidence fairly strong integration with the polymer matrix.
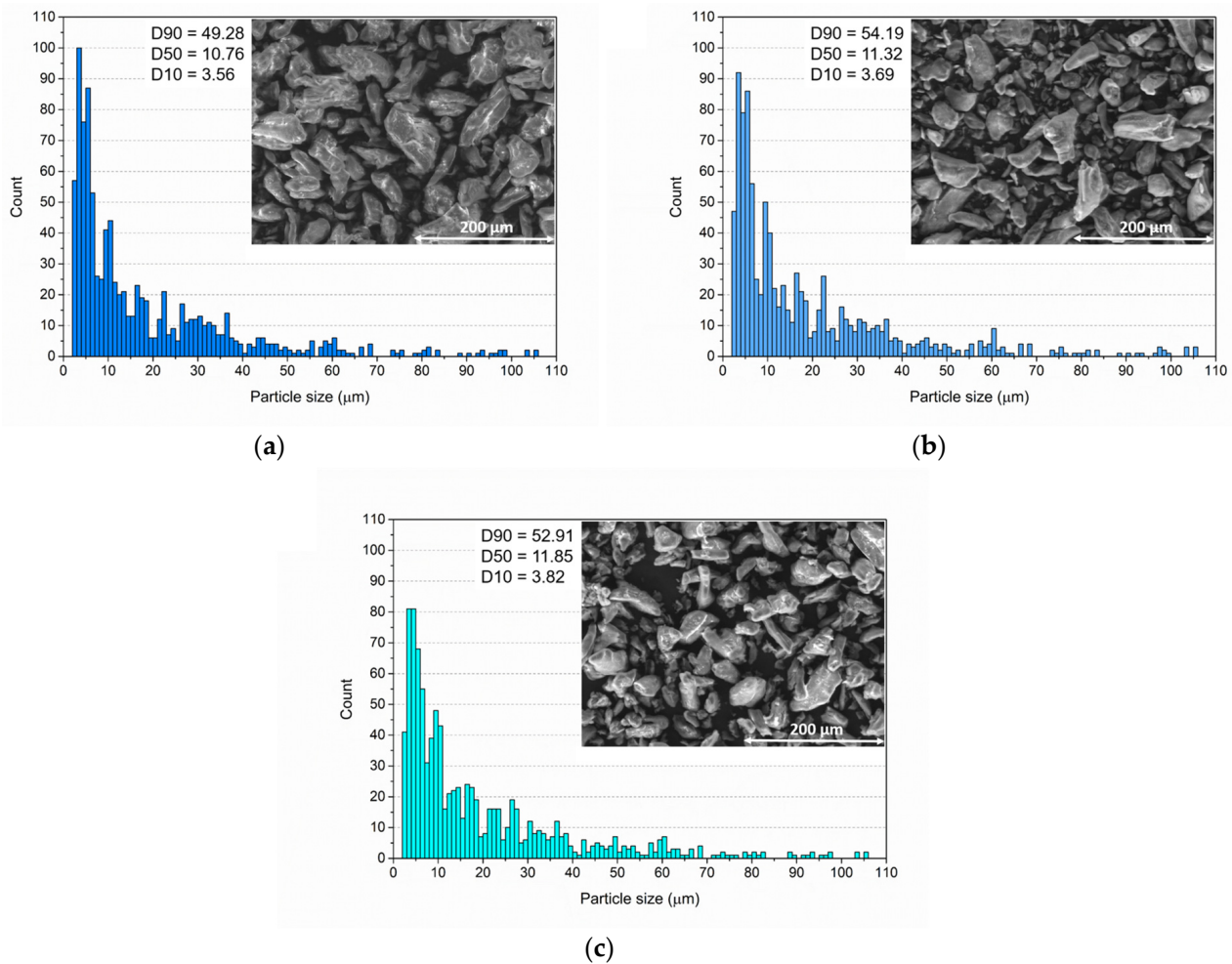

(**a**)

(**b**)

(**c**)

Figure 1. Size distribution analysis carried out with ImageJ on (**a**) olive pit powder, (**b**) olive pit powder functionalized with silane, and (**c**) olive pit powder functionalized with wax. The pictures of the powders were acquired by SEM (scale bar: 200 μm).
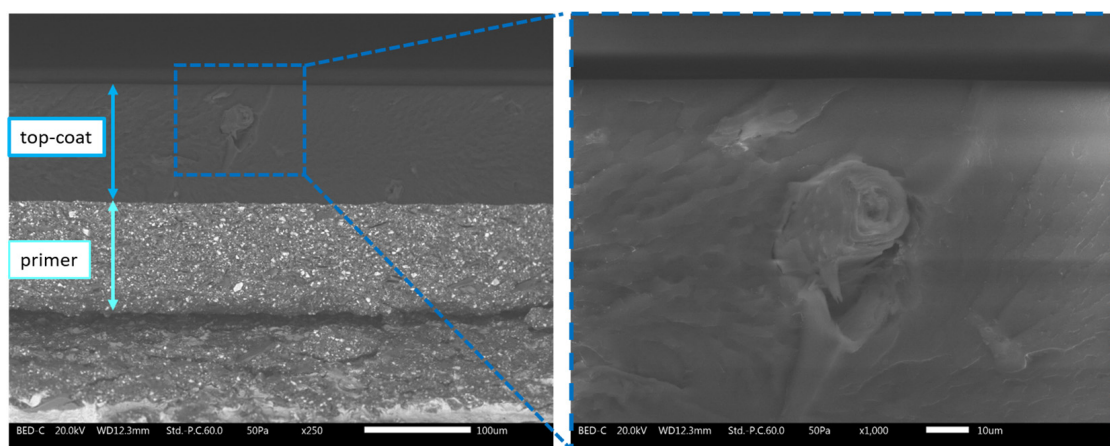

Figure 2. SEM micrograph of the cross-section of coating S, with the enhancement of an olive pit granule embedded inside the top coat.

Regardless of the functionalization process of the powder, the granules exhibit a solid interaction with the polyurethane matrix of the top coat. In fact, the images in Figure 2 are just one example of the excellent interconnection between powder and paint matrix, observed in all three series of samples O, S, and W. Therefore, the powders deriving from olive pits are candidates for applications as filler/pigment in spray paints, thanks to an excellent mixing with the paint and a good compatibility with the organic matrix of the coating.

This aspect is highlighted even better by the images in Figure 3. The appearance of samples O, S, and W is markedly different from that of sample T, which is free of bio-based filler, both at the macro- (left) and microscopic (right) levels. The granules, homogeneously dispersed in the top coat, provide a specific color to the coating. The functionalization of the powders does not cause an evident color change in the granules, as the three samples O, S, and W appear identical to each other.
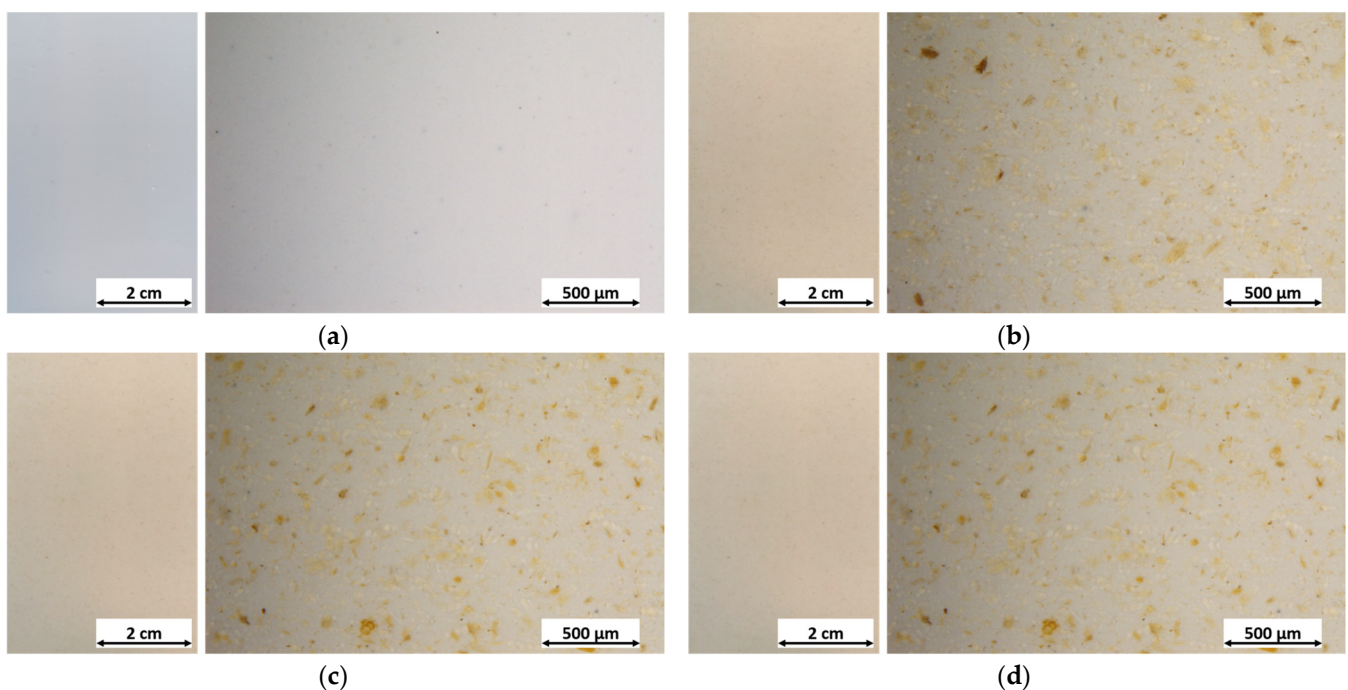

Figure 3. Top view micrographs of (**a**) sample T, (**b**) sample O, (**c**) sample S, and (**d**) sample W.

The colorimetric analyses in Figure 4 emphasize this feature, as the graph shows the total color variation ΔE of the three samples containing the bio-based fillers compared to the reference coating T. The ASTM E308 (2018) standard [61] expresses total color variation ΔE as:

$$\Delta E = [(\Delta L^*)^2 + (\Delta a^*)^2 + (\Delta b^*)^2]^{1/2} \tag{1}$$

where the colorimetric coordinates L*, a*, and b* represents the lightness (0 for black and 100 for white objects), the red-green coordinate (positive values are red, negative values are green, and zero as neutral parameter), and the yellow-blue coordinate (yellow for positive values, blue for negative values, and zero as neutral parameter), respectively.

The color change caused by the fillers is easily recognizable, as the average values of E are around 12 for all three samples. As a color change with an E value of 1 is defined in the literature as being perceptible even to the human eye [62,63], the samples O, S, and W appear very different from the coating T, as stressed in Figure 3. In addition to the mean value of ΔE, the error bars are also very similar between the three samples containing the filler, proving that the functionalization process does not affect the appearance of the granules.
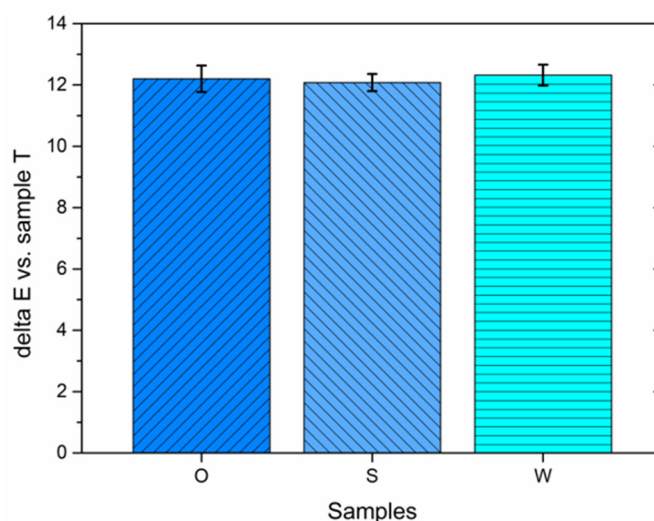
Figure 4. Change in appearance of the samples due to the contribution of the bio-based granules.

Table 2 exhibits the evolution of the colorimetric coordinates of the four series of samples. The addition of the filler acts on all three colorimetric coordinates. The brightness of the coating is reduced, as the granules cause a decrease in the coordinate L* of about 5–6 points. This is accompanied by a slight growth of the coordinate a* (with a tendency towards red), but above all a clear increase in the value of b*, a symptom of a concrete shift towards yellow tones.

Table 2. Colorimetric coordinates of the four series of samples.

Sample	L*	a*	b*
T	93.51	−0.85	3.17
O	87.50	−0.06	13.76
S	88.30	−0.06	14.04
W	87.96	−0.03	14.14

Ultimately, the olive pit powders can be applied as pigment for paints, notably affecting the appearance of the coating, regardless of whether they are subjected to a functionalization process or not.

3.2. Effect of Olive Pit Functionalization on Paint Durability

The olive pit powders are an ideal choice for a versatile pigment for water-based paints applied by spray deposition due to their great coloring ability. However, a recent work [43] highlighted some critical issues related to the application of the untreated olive pit powder into paints. The addition of the granules into the waterborne paint have resulted in the loss in the coating's ability to protect against harsh environments, due to the lignocellulose and hydrophilic nature of the olive pit powder [43]. For this reason, the powders employed in this study were functionalized with silanes and wax to verify whether the surface conversion process of the granules was able to reduce or even avoid these problems, without compromising the protective performance of the paint. Thus, the four series of samples were subjected to different accelerated degradation tests and electrochemical analyses to assess the role of the functionalization process on the protective features of the filler.

3.2.1. Salt Spray Test

Throughout the first 100 h of exposure in the salt spray chamber, the samples were checked every 24 h. Until the test's conclusion, the samples were checked every 100 h. An artificial notch with a width of 1 mm was produced on the surface of the coatings with the

intention of inducing the development of corrosive phenomena at the substrate–coating interface. During the monitoring of the behavior of the samples, both the blister evolution phenomena and the coating delamination processes at the notch were considered [64].

Figure 5 depicts the changes in the coatings' appearance while they were subjected to the salt spray chamber's exposure. The aggressive atmosphere in the chamber inevitably caused degradation phenomena in the four series of samples. Corrosion products developed form the notch, as it exposed the steel substrate to the chemical attack of the chloride-rich test solution. Moreover, the solution absorption at the coating–substrate interface in the proximity of the scratch gave rise to the growth of blisters. Finally, the paint's inherent porosity encouraged the development of water uptake phenomena even far from the simulated defect.
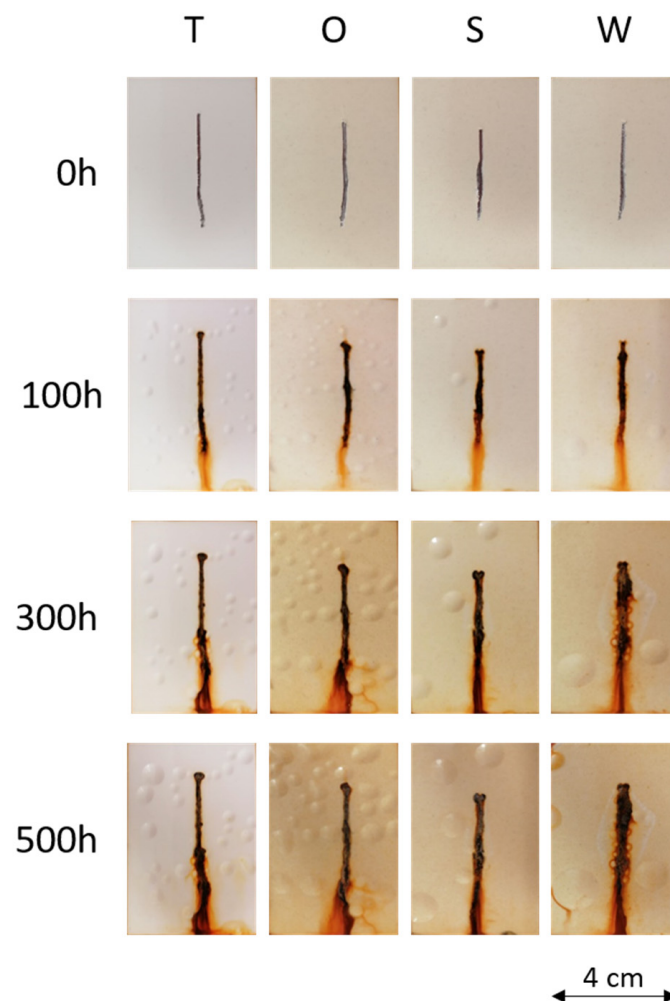

Figure 5. Coatings' degradation during the exposure in salt spray chamber.

Although these occurrences were observed on all sample series, the three different types of fillers played a key role in the development of the blisters, and consequently on the barrier effect of the composite coating. The images in Figure 5 show a real difference in behavior between the four samples, but the graphs in Figure 6 better highlight the effect of bio-based fillers on the durability of the paint. While Figure 6a shows the growth of the number of blisters during salt spray chamber exposure, Figure 6b reveals the percentage area of the coatings covered by these defects.
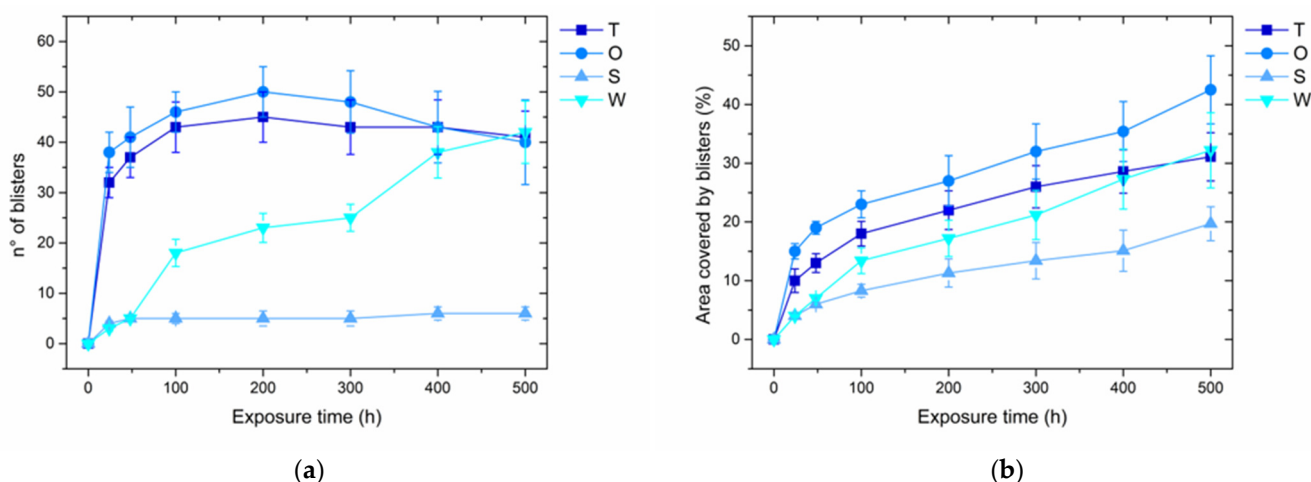
Figure 6. Evolution of (**a**) the number of blister and (**b**) the surface covered by blister during sample exposure in salt spray chamber.

Sample T shows a very rapid development of blisters, as a symptom of a limited barrier effect of the waterborne paint. After 100 h, no new blisters rise, but the already existing ones continue to grow in size, covering more and more surface area of the sample. The untreated olive pit powder (sample O) causes an exacerbation of this phenomenon, with a greater number of blisters and area conditioned by the defects. Furthermore, the decrease in blisters observed after 200 h is due to the union of several bulges that come into contact, to form large protuberances, even up to 5000 μm. This phenomenon had already been observed in the previous work [43] and is mainly due to the hydrophilic lignocellulose nature of the olive pit [41,44,45], which promotes undesired water uptake occurrences [65,66]. With the aim of masking the hydrophilic characteristic of the filler, the powders were functionalized with silanes and wax. Indeed, the silane seems to considerably improve the behavior of the granules (sample S). The blisters increase in size over time but are very limited in number. Therefore, the defectiveness of the coating is greatly limited by the functionalized filler, which even improves the barrier effect of the polyurethane matrix. On the other hand, the wax (sample W) involves a reduction in the number of blisters compared to the filler-free coating (sample T), but they still increase considerably in size. Furthermore, during the test, several blisters develop at the notch, representing an ineffective barrier, such as that evidenced by the silane-treated powders.

Figure 7 shows a focus of the notch of the samples after 500 h of exposure in the salt spray chamber. Despite the good protective behavior of the functionalized powders, the development of corrosion products in proximity of the artificial defect favors cathodic delamination phenomena in all four series of samples. In this case, in the presence of a large defect, the powders are unable to limit the phenomenon of cathodic delamination. The effective detachment of the four types of coating even reaches 5000 μm away from the notch. The coatings do not exhibit significant adhesion properties since the norm specifies 1000 μm as the maximum threshold for the detachment distance from the cutting region [52].

Therefore, the surface conversion process of the olive pit powders, and in particular the one with silane, seems to lead to a reduction of the hydrophilic features of the filler, with a consequent improvement in the protective performance of the paint, only on the condition that the coating is intact. The presence of a macroscopic defect, such as the artificial notch shown in Figures 5 and 7, in fact, compromises and nullifies the protective properties of the filler. Ultimately, the study demonstrates that the correct functionalization of the powders can ensure their application as a bio-based pigment and protective filler in water-based paints. However, it is necessary to pay attention to the integrity of the coating itself, which must necessarily possess limited defectiveness, in order to best exploit the protective contribution of the functionalized granules.
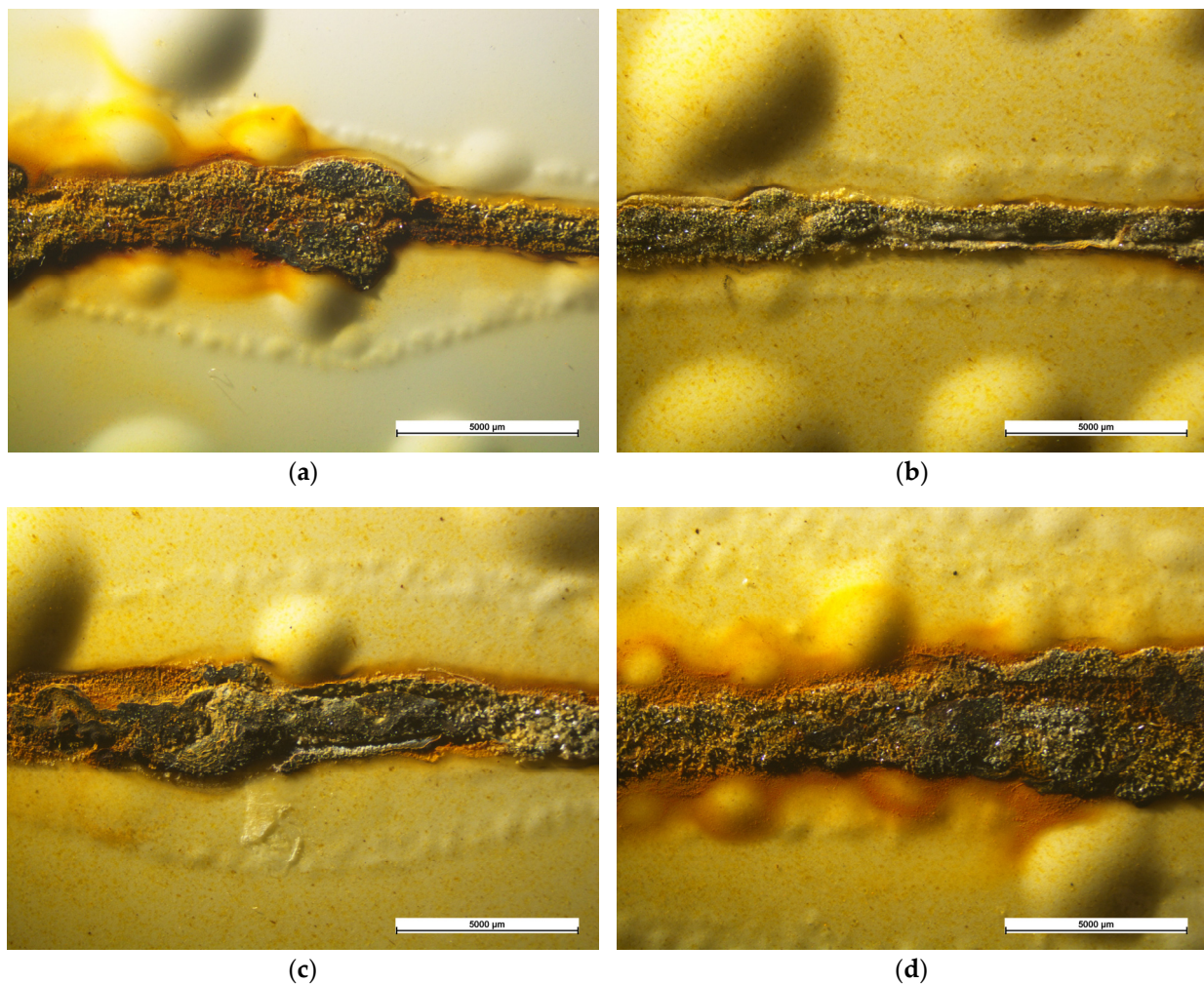
Figure 7. Cathodic delamination at the artificial notch of (**a**) sample T, (**b**) sample O, (**c**) sample S, and (**d**) sample W, after 500 h of exposure in the salt spray chamber.

3.2.2. Contact Angle Measurements and Paint Liquid Resistance

With the aim of better analyzing the water repellency characteristics of the surface of the coatings and to assess in detail the hydrophobic role of the functionalized powders, the samples were subjected to apparent contact angle measurements and liquid resistance test.

Since the samples' exposure in the salt spray chamber revealed positive behavior due to the presence of functionalized fillers, the wettability of the surfaces was firstly investigated to understand whether the protective contribution of the powders was mainly superficial. The results of the wettability test are tabulated in Table 3, and represent the average of 10 measurements per sample, while Figure 8 shows some images acquired during the measurements. Since the size of the drop is considerably greater than the surface and morphological irregularities of the coatings, those measured and expressed in Table 3 and in Figure 8 represent the apparent and not actual contact angle values. The test does not show a clear difference in behavior between the four sets of samples. The degree of wettability of the paint does not seem to be significantly influenced by the presence of fillers. However, the untreated powder (sample O) causes a slight decrease in the apparent contact angle, due to the hydrophilic nature of the olive pit. The angle values increase again in the presence of functionalized powders (samples S and W) to achieve results similar to the reference paint (sample T).

Table 3. Contact angle measurements (θ).

Sample	θ (°)
T	75 ± 4
O	71 ± 1
S	76 ± 3
W	80 ± 5
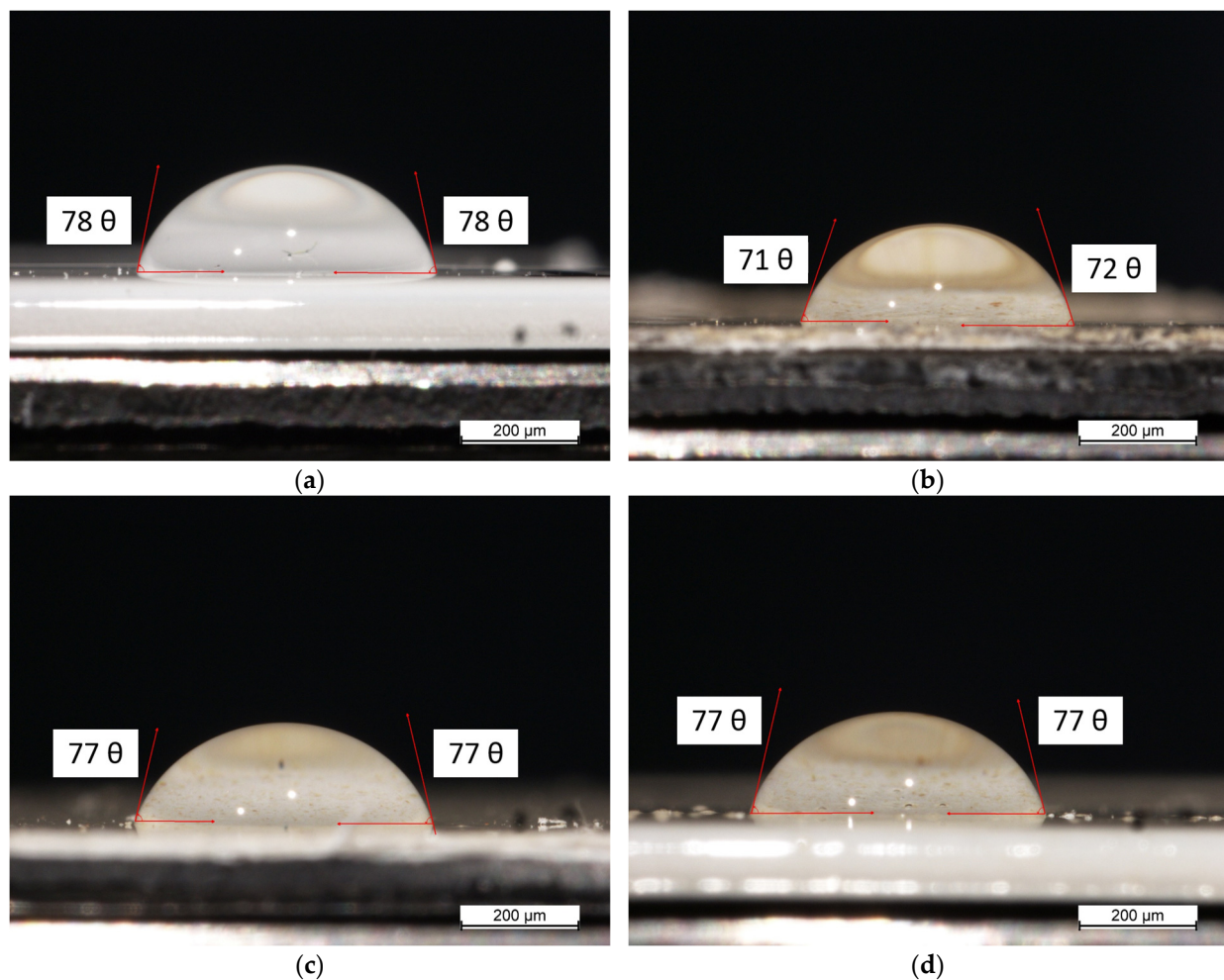
Figure 8. Contact angle measurements of (**a**) sample T, (**b**) sample O, (**c**) sample S, and (**d**) sample W.

The results indicate that the bio-based filler does not offer a protective contribution at the 'superficial' level. The presence of powders nearby the surface of the coating is probably so low that it cannot act significantly on the wettability values of the coating. The concentration of filler equal to 2 wt.%, despite being high in absolute terms, is not sufficient for an adequate distribution of powder to be present on the surface of the layer. Therefore, the results expressed by the salt spray chamber exposure test are mainly due to the contribution of the filler within the bulk of the coating. However, the slight difference between the apparent contact angles of the samples S and W, with respect to coating O, suggests that the functionalization process has an effective hydrophobic contribution, which is observable even in the presence of small amounts of powder in proximity of the layer external surface.

To better analyze the behavior of the filler on a macroscopic level, the samples were subjected to the liquid resistance test. In fact, the literature suggests employing the liquid resistance test to evaluate the effect of certain fillers, whether they are pigments [67,68] or multifunctional powders [69], on the barrier properties of waterborne paints. Figure 9

summarizes the results of the chemical resistance test carried out on the four series of samples, which were evaluated considering their color change. The values included in the graph represent the degree of discoloration of the paint due to the contact with the liquid, whose relationship with the color change is explained in the Table 4 [70]. The paint performs better the lower its rating for chemical resistance.
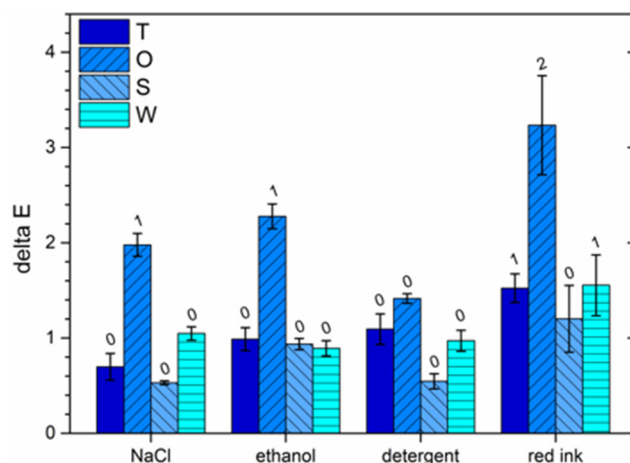

Figure 9. Coatings color changes of the samples after contact with liquids. The numbers above the columns are representative of the levels in Table 4.

Table 4. Color difference values corresponding to the level of discoloration.

Level	Degree of Discoloration	Color Difference
0	no discoloration	≤ 1.5
1	very slight fading	1.6–3.0
2	slight color change	3.1–6.0
3	apparent discoloration	6.1–9.0
4	severe color change	9.1–12.0
5	complete discoloration	>12.0

The graph in Figure 9 reveals and confirms a clearly evident behavior: the untreated powder (sample O), with its hydrophilic nature, favors the absorption and penetration of the liquid inside the coating, leading to a significant color change in some cases. In fact, the values of ΔE of sample O are always higher of that of the reference coating T. On the other hand, the functionalized powders cause a reduced color change, confirming the good hydrophobic behavior exerted by the silane and the wax. Specifically, once again, the powder functionalized with silane (sample S) shows the best behavior, with color change values ΔE lower than the pure polyurethane paint (sample T).

The two tests, namely the contact angle measurements and the liquid resistance test, reveal the contribution of the surface conversion process of the olive pit powders in reducing their undesired hydrophilic characteristics. The results confirm and validate the output of the exposure of the samples in the salt spray chamber, highlighting the excellent behavior of the powders functionalized with silane.

3.2.3. UV-B Exposure

Despite the UV light can results in the photo-oxidative degradation of the polymer [71], waterborne polyurethane-acrylate materials based on aliphatic isocyanate provide strong protection against the chemical-physical degradation caused by UV light [72,73]. Otherwise, the main components of the olive pit, lignin and cellulose, tend to degrade significantly when exposed to sunlight [74,75]. As a matter of fact, the previous study on the use of different concentrations of olive pit powder had highlighted a high degradation phenomenon of the lignin- and cellulose-based filler when exposed to UV-B radiation [43]. Furthermore, this powder decay process was associated with the absorption into the coating of the

moisture present in the UV chamber, due to alternating cycles of UV-B radiation and vapor condensation atmosphere. Consequently, the same exposure test was performed with the four series of samples of this study, verifying the protective behavior of the functionalized filler when subjected to stresses that could lead to its chemical degradation.

Figure 10 exhibits the changes of the FTIR spectra of the four samples during the exposure to UV-B light. Figure 10a shows the spectra of the pure polyurethane–acrylate matrix (sample T), free of any bio-based filler. The absorption band between 3400 and 3300 cm^{-1} corresponds to the stretching vibration of the NH bond, as characteristic of urethane and urea groups. The stretching region between 3000 and 2800 cm^{-1} is correlated to the –CH and –CH_2 groups, while the two intense peaks at about 1724 and 1683 cm^{-1} can be assigned to the typical carbonyl absorption band and the urethane and urea carbonyl groups, respectively [76]. The band at 1529 cm^{-1} is associated to the N-H deformations [77], while the peaks at 1460 and 1378 cm^{-1} refer to the bending of CH_2 aliphatic. The signals at 1238 and 1142 cm^{-1} can be attributed to N-H bending and to the coupled C-N and C-O stretching vibrations. Finally, the peaks at 843 and 764 cm^{-1} represent the C-H stretching and to the ester C-O-C symmetric stretching vibration, respectively [78]. As the acryl-polyurethane paint is based on water-soluble acrylic-modified resins and aliphatic isocyanate, coating T is not affected by the exposure to UV radiation [43]. Thus, the spectra of sample T did not evolve during the accelerated degradation test.
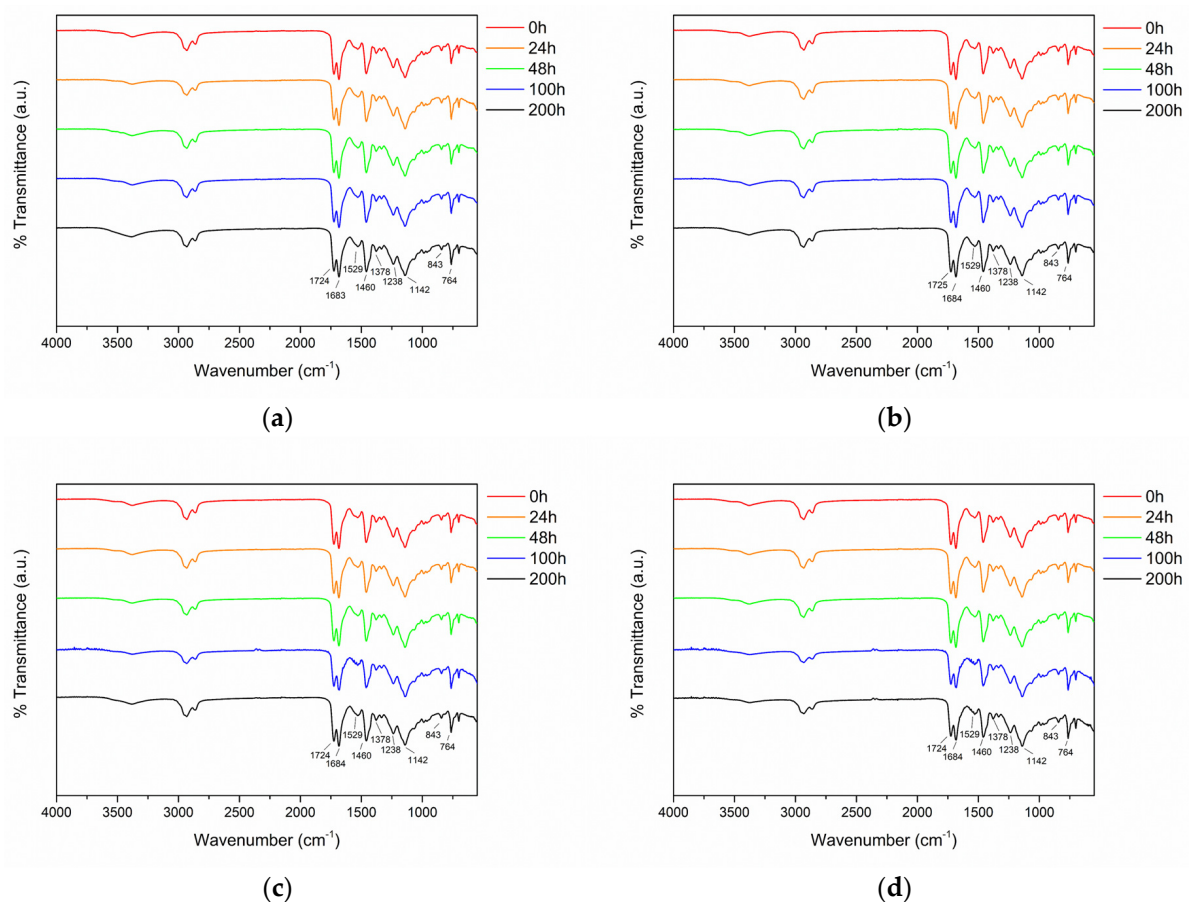

Figure 10. Evolution of the FTIR spectra of (**a**) sample T, (**b**) sample O, (**c**) sample S, and (**d**) sample W, during the exposure to UV-B radiation.

As observed in the previous work [43], the amount of filler introduced into the paint cannot be appreciated by FTIR analysis. Consequently, the spectra of samples O, S, and W are quite similar to those of samples T, as the peaks related to the lignocellulose materials are exact duplicates of those in the polymer matrix. The absorption band between 3400 and

3300 cm^{-1} is attributed to the stretching vibration of the -OH group [79]. Differently, the stretching region between 3000 to 2800 cm^{-1} corresponds the -CH group of cellulose, hemicellulose, and lignin [80]. The signal at around 1700 cm^{-1} can be assigned to the stretching vibrations of the unconjugated C=O group and specific moieties of the polymeric chains present in the lignocellulose, such as esters [81]. The band at 1460 and 1530 cm^{-1} represent the C-H deformation vibration and aromatic skeletal vibration of lignin, respectively [82]. Finally, the peak at 1238 cm^{-1} is attributed to the C-O stretching. Since the spectra of the three samples containing the bio-based fillers did not undergo changes during the test, the infrared analyses could suggest an excellent durability and resistance to ultraviolet radiation of the coatings O, S, and W.

However, the colorimetric inspections of Figure 11 reveal a high color change ΔE of these three samples during exposure to UV-B radiation. While the polymeric matrix (sample T) did not undergo considerable alterations, the lignin-based fillers show a rapid color change, which causes the concrete modification of the appearance of the three coatings O, S, and W. After all, the photo-oxidation occurrence of the wooden material, which constitutes the olive pit filler, was predictable [43]. The functionalization process with silane or wax does not alter this degradation process of the filler, and consequently, it is not possible to appreciate a difference in behavior between the three samples O, S, and W.
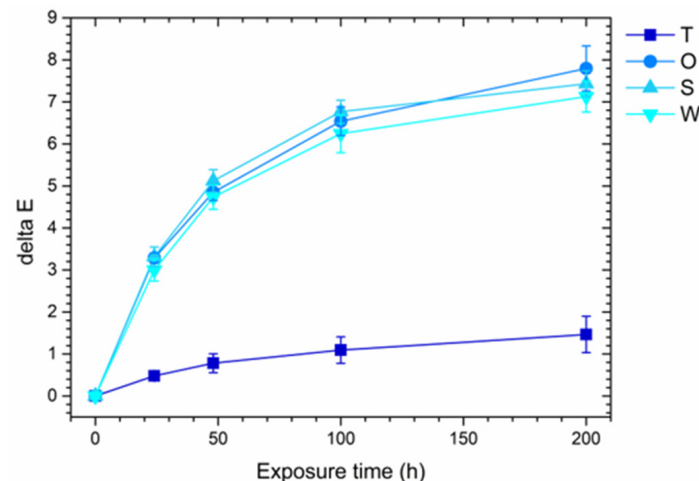

Figure 11. Total color variation during UV-B exposure.

Again, the performance of these three samples is distinguished by the hydrophilic/hydrophobic characteristics of the bio-based filler they contain. UV radiation was alternated with condensed vapor exposure cycles in order to observe possible water uptake phenomena facilitated by the physical-chemical degradation of the polymer matrix and fillers. The result of these phenomena is highlighted in Figure 12, which reveals the evolution of the number and dimension of blisters in the samples (Figure 12a and Figure 12b, respectively) during the test.

The water uptake occurrence took place very quickly, mainly during the first 50 h of the experiment. Compared to the pure polymeric matrix (sample T), the untreated olive pit granules (sample O) caused the development of a greater number of blisters of smaller dimensions. This event arises due to the hydrophilic nature of the lignocellulose filler, whose granules represent sites of easy permeation of humidity in the polyurethane matrix. Otherwise, although samples S and W have slightly larger blisters, their number is drastically reduced, confirming the good hydrophobic behavior of functionalized fillers. The entire water uptake phenomenon is restricted to limited spots, as the filler exerts a good barrier effect, improving the performance of the polyurethane matrix.
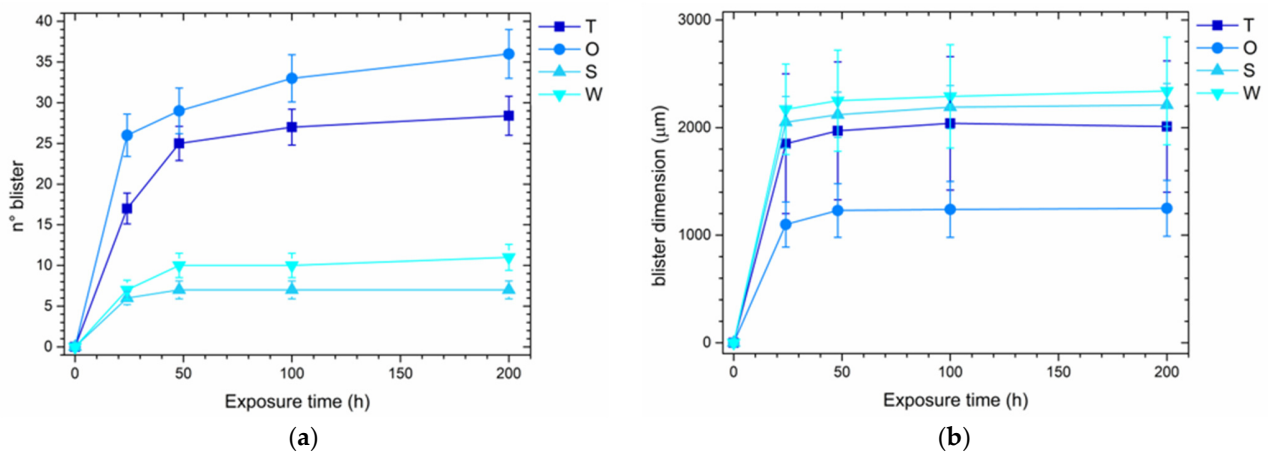
(**a**)　　　　　　　　　　　　　　　　　　　(**b**)

Figure 12. Evolution of (**a**) the number and (**b**) the dimension of blisters developed during UV-B exposure.

Finally, Figure 13 shows the morphology of the blister observed in the four samples at the end of the test. Sample S still confirms the best performance, as the blisters are slightly smaller in size and number than those of sample W. This is further confirmation of the greater effectiveness of the surface conversion process of the granules using silane, rather than wax. The industrial functionalization process does not avoid the photo-oxidative degradation of the lignocellulose material, as evidenced by the color change in Figure 11, but it is still able to reduce the water uptake occurrence due to the hydrophilic nature of the olive pit.
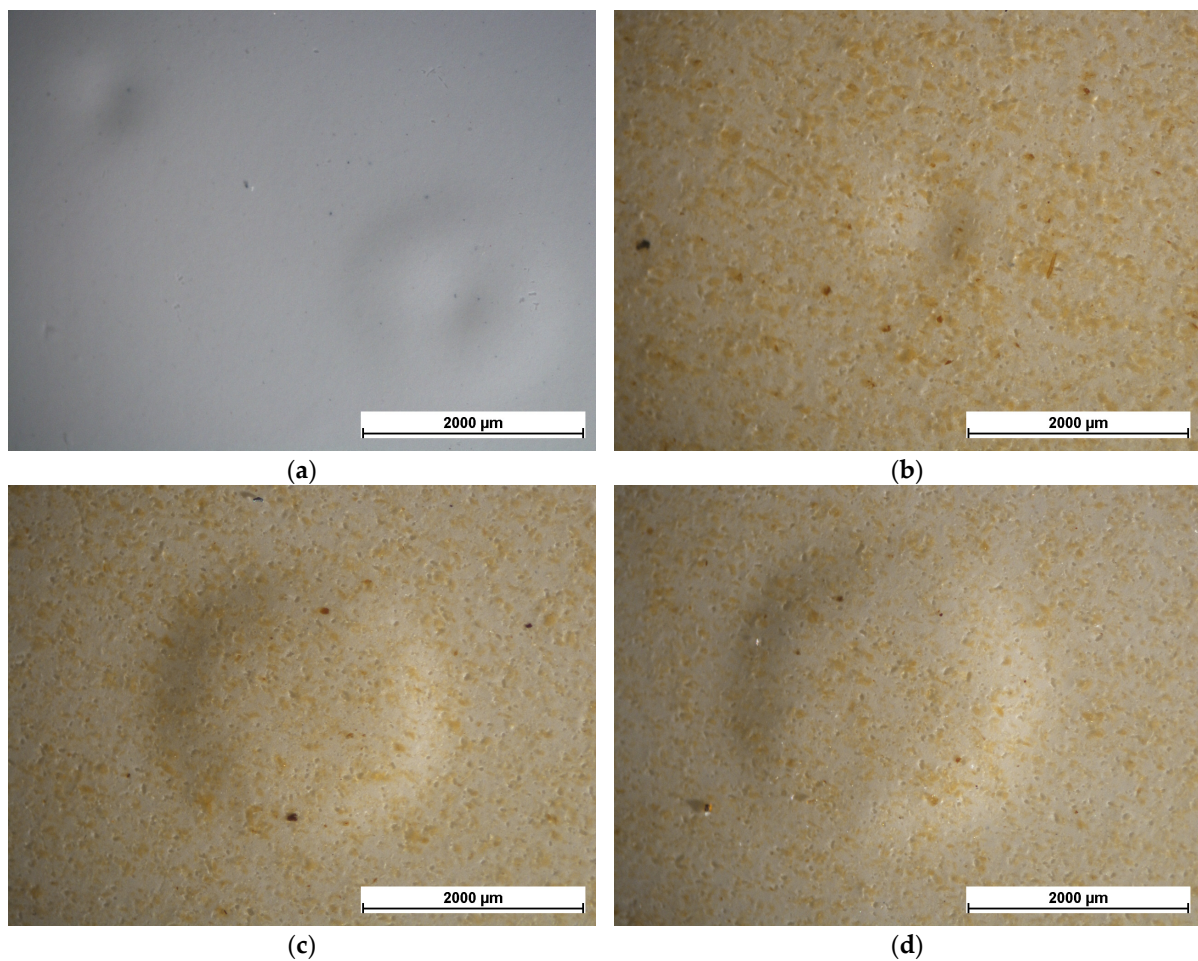

(**a**)　　　　　　　　　　　　　　　　　　　(**b**)

(**c**)　　　　　　　　　　　　　　　　　　　(**d**)

Figure 13. Blister appearance of (**a**) sample T, (**b**) sample O, (**c**) sample S, and (**d**) sample W, after 200 h of exposure to UV-B radiation.

3.2.4. Electrochemical Impedance Spectroscopy

Electrochemical Impedance Spectroscopy (EIS) measurements are widely used to assess the protective properties of paints [83], evaluating their defectiveness or degree of adhesion [84]. The Bode impedance moduli measured at low frequencies (10^{-2} Hz), defined as $|Z|_{(0.01)}$, is a parameter which gives a rough quantitative estimate of the level of protection the coating affords. Various literature works define the $|Z|_{(0.01)}$ value as 10^6 $\Omega \cdot cm^2$ as the lower limit for defining a coating as 'protective' [85].

Thus, the protective behavior of the four series of coatings was evaluated by recording the development of their impedance module $|Z|_{(0.01)}$ over time. Figure 14 depicts the change in the parameter $|Z|_{(0.01)}$ over the course of the samples' 500-hour exposure to the test solution. Since all four samples show $|Z|_{(0.01)}$ values that never fall below the threshold limit of 10^6 $\Omega \cdot cm^2$, the test result suggests that the coatings of the four series provide adequate protection to the steel substrate. In confirmation of the previous results, the powders functionalized with silane of sample S seem to offer greater protective guarantees than the other types of fillers (samples O and W). However, the graph shows an unexpected trend: while the three coatings containing the fillers show a decrease of $|Z|_{(0.01)}$ over time, typical of an organic layer, the sample T exhibits an increase of the impedance modulus during the measurements. This result does not represent a better protective feature of the pure polyurethane matrix of the coating T, but rather suggests that the layer has poor adhesion, and the penetration of test solution into the polymeric matrix favors bulging phenomena. The tendency for solution absorption and the resultant production of corrosion products increases the resistive effect of the system. This phenomenon falsifies the result of the EIS measurements but highlights a poor protection of the coating when in contact with an aggressive solution.
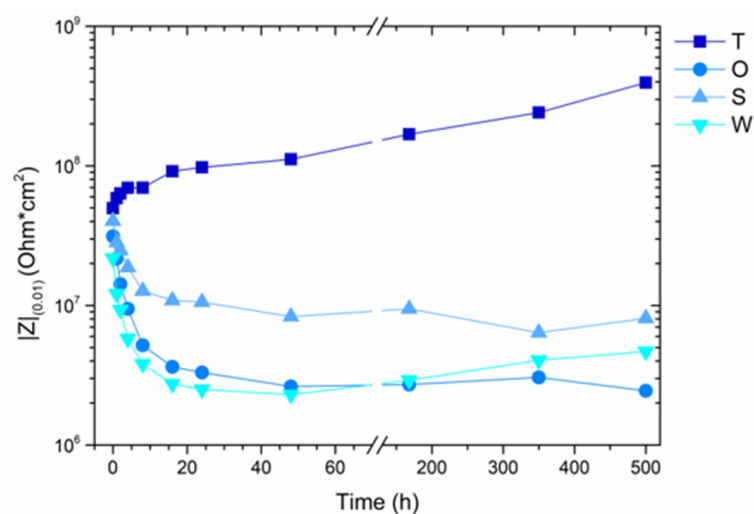

Figure 14. Bode impedance modulus $|Z|_{(0.01)}$ evolution with time.

To better analyze the behavior of the four samples and explain the results exhibited in Figure 14, the evolution of the Bode phase spectra is displayed in Figure 15. The spectrum at t = 0 h of Figure 15a (sample T) highlights a single asymmetric broad peak, representing the high-frequency time constant, associated to the dissipation phenomena that occur through the coating [86]. Already after 24 h, a shoulder at low frequency ($\approx 10^0$ Hz) develops. This outcome is representative of a second low-frequency time constant that is typical of the reactions at the coating–substrate interface. Once more, this second time constant points to a non-trivial issue in the layer. Furthermore, the peak grows in size over time, a symptom of a dissipation process at the substrate interface that is constantly evolving during the test. Figure 15b (sample O) shows a clearer and more standard trend. Already at the beginning of the test, two well-defined and isolated peaks were observed, representative of the two time constants. Therefore, the system is immediately affected by the defects

of the coating, represented by the second time constant ($\approx 10^0$ Hz). Subsequently, this low-frequency time constant disappears, and the curves shift towards high-frequency values. These occurrences allude to a decrease in the coatings' insulating abilities as a result of the absorption of solution into the layer, along with associated dissipative phenomena that take place at the metal's surface. Therefore, even the coating O does not seem to offer good protective guarantees, as already highlighted by the previous tests. The situation is different for sample S and sample W (Figure 15c and Figure 15d, respectively). The trend of the spectra is typical of a protective coating: a single time constant curve at high frequencies, which shifts over time towards higher frequencies [87]. Although very similar, the curves of the sample S exhibit a smaller shift over time, confirming the better protective performance of the coating containing the powders functionalized with silane.
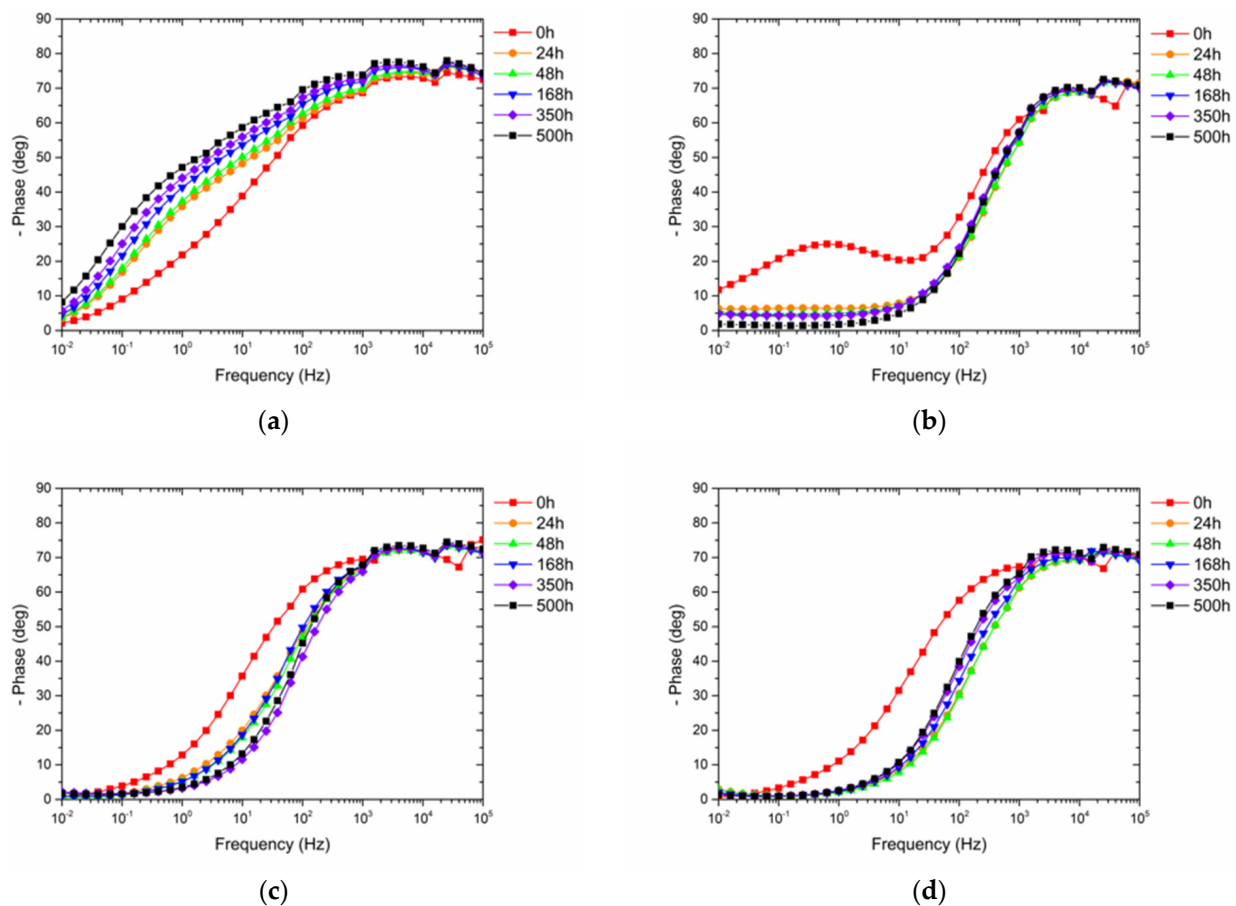

Figure 15. Bode phase spectra evolution with time of (**a**) sample T, (**b**) sample O, (**c**) sample S, and (**d**) sample W.

Ultimately, the impedance measurements confirm what has already been observed: the importance of the bio-based filler surface conversion process. The untreated powders do not represent a protective filler, as their hydrophilic nature facilitates the absorption of solution into the polymeric matrix. Conversely, the treatment with silane, even more than with wax, increases the hydrophobicity of the granules, with a consequent improvement in the barrier performance of the composite coating.

4. Conclusions

This work highlights the effectiveness of the functionalization of olive pit granules, with the aim to increase their hydrophobicity and improve their protective performance as green filler for eco-sustainable paints. The untreated bio-based filler, which can be applied as multifunctional pigment, has several issues related to its hydrophilic nature.

Conversely, the powders treated with silane and wax significantly increase the durability of the composite coating.

The functionalization process does not modify the morphology of the filler, nor does it affect its compatibility with the polymeric matrix of the coating. In fact, the granules exhibit a solid interaction with the polymeric matrix, as well as after the fragile nitrogen fracture processes. Furthermore, the aesthetic features and the coloring power of the granules are not negatively influenced by the surface conversion treatments with silane and wax. Thus, the color coordinates of the three coatings containing the bio-based filler have almost identical values, and the appearance of the three series of layers cannot be distinguished by eye.

The increase in hydrophobicity of the filler exerted by the silane and the wax causes a reduction in the water uptake phenomena of the samples exposed in the salt spray chamber, which results in a decrease in the number and size of blisters developed during the test. However, this phenomenon occurs in the case of intact coatings: the presence of macroscopic defects, in fact, compromises and nullifies the protective properties of the filler.

Although the macroscopic level of surface hydrophobicity of the coating is not concretely reduced by the functionalized filler, as evidenced by the contact angle measurements, the tests of resistance to liquids of the paints show a fundamental role of the two functionalized powders in mitigating the absorption of the test solutions. The wax and the silane considerably reduce the discoloration phenomenon that the untreated olive pit granule undergoes in contact with the test liquids.

The industrial functionalization process does not avoid the photo-oxidative degradation of the lignocellulose material when exposed to UV radiation, but it is still able to reduce the water uptake phenomena in the paint. Specifically, silane, even more than wax, proves to be able to reduce the number and size of blisters due to the absorption of humidity in the polymeric matrix, despite the evident decay of the lignocellulose filler.

Finally, the impedance measurements highlight the importance of the bio-based filler surface conversion process in increasing the hydrophobicity of the granules, with the consequent improvement of the barrier performance of the composite coating. The silane causes an increase of an order of magnitude of the impedance modulus $|Z|_{(0.01)}$ compared to the untreated filler, even after prolonged contact (500 h) with the test solution.

In conclusion, the work demonstrates how it is actually possible to use waste from the agro-food industrial field as a filler in eco-sustainable paints, through suitable surface conversion processes that increase its hydrophobicity and consequently improve its protective performance. The treatment with silane, even more than with wax, shows the best result and is proposed as an effective material for the surface conversion of lignocellulose fillers.

References

1. Ortega, F.; Versino, F.; López, O.V.; García, M.A. Biobased composites from agro-industrial wastes and by-products. *Emergent Mater.* **2022**, *5*, 873–921. [CrossRef]
2. Razza, F.; Briani, C.; Breton, T.; Marazza, D. Metrics for quantifying the circularity of bioplastics: The case of bio-based and biodegradable mulch films. *Resour. Conserv. Recycl.* **2020**, *159*, 104753. [CrossRef]
3. Richard, S.; Rajadurai, J.S.; Manikandan, V. Influence of particle size and particle loading on mechanical and dielectric properties of biochar particulate-reinforced polymer nanocomposites. *Int. J. Polym. Anal.* **2016**, *21*, 462–477. [CrossRef]
4. Mustapha, R.; Rahmat, A.R.; Abdul Majid, R.; Mustapha, S.N.H. Vegetable oil-based epoxy resins and their composites with bio-based hardener: A short review. *Polym. Plast. Technol. Mat.* **2019**, *58*, 1311–1326. [CrossRef]
5. Sadh, P.K.; Duhan, S.; Duhan, J.S. Agro-industrial wastes and their utilization using solid state fermentation: A review. *BIOB* **2018**, *5*, 1. [CrossRef]
6. Binoj, J.; Raj, R.E.; Daniel, B. Comprehensive characterization of industrially discarded fruit fiber, *Tamarindus indica* L. as a potential eco-friendly bio-reinforcement for polymer composite. *J. Clean. Prod.* **2017**, *142*, 1321–1331. [CrossRef]
7. Sanjay, M.; Madhu, P.; Jawaid, M.; Senthamaraikannan, P.; Senthil, S.; Pradeep, S. Characterization and properties of natural fiber polymer composites: A comprehensive review. *J. Clean. Prod.* **2018**, *172*, 566–581. [CrossRef]
8. Satyanarayana, K.G.; Arizaga, G.G.; Wypych, F. Biodegradable composites based on lignocellulosic fibers—An overview. *Prog. Polym. Sci.* **2009**, *34*, 982–1021. [CrossRef]
9. Gurunathan, T.; Mohanty, S.; Nayak, S.K. A review of the recent developments in biocomposites based on natural fibres and their application perspectives. *Compos. Part A Appl. Sci.* **2015**, *77*, 1–25. [CrossRef]
10. Vandamme, E.J. Agro-industrial residue utilization for industrial biotechnology products. In *Biotechnology for Agro-Industrial Residues Utilisation*; Springer: Berlin/Heidelberg, Germany, 2009; pp. 3–11.
11. Balasundar, P.; Narayanasamy, P.; Senthil, S.; Al-Dhabi, N.A.; Prithivirajan, R.; Kumar, R.S.; Ramkumar, T.; Bhat, K.S. Physico-chemical study of pistachio (Pistacia vera) nutshell particles as a bio-filler for eco-friendly composites. *Mater. Res. Express* **2019**, *6*, 105339. [CrossRef]
12. Andrew, J.J.; Dhakal, H. Sustainable biobased composites for advanced applications: Recent trends and future opportunities–A critical review. *Compos. Part C Open Access* **2022**, *7*, 100220. [CrossRef]
13. Arias, J.; Fernandez, M. Biomimetic processes through the study of mineralized shells. *Mater. Charact.* **2003**, *50*, 189–195. [CrossRef]
14. Toro, P.; Quijada, R.; Yazdani-Pedram, M.; Arias, J.L. Eggshell, a new bio-filler for polypropylene composites. *Mater. Lett.* **2007**, *61*, 4347–4350. [CrossRef]
15. Yew, M.; Sulong, N.R.; Yew, M.; Amalina, M.; Johan, M. The formulation and study of the thermal stability and mechanical properties of an acrylic coating using chicken eggshell as a novel bio-filler. *Prog. Org. Coat.* **2013**, *76*, 1549–1555. [CrossRef]
16. Pradhan, A.K.; Sahoo, P.K. Synthesis and study of thermal, mechanical and biodegradation properties of chitosan-g-PMMA with chicken egg shell (nano-CaO) as a novel bio-filler. *Mater. Sci. Eng. C* **2017**, *80*, 149–155. [CrossRef] [PubMed]
17. Wang, F.; Liu, H.; Yan, L. Comparative Study of Fire Resistance and Char Formation of Intumescent Fire-Retardant Coatings Reinforced with Three Types of Shell Bio-Fillers. *Polymers* **2021**, *13*, 4333. [CrossRef]
18. Yew, M.C.; Yew, M.K.; Saw, L.H.; Ng, T.C.; Durairaj, R.; Beh, J.H. Influences of nano bio-filler on the fire-resistive and mechanical properties of water-based intumescent coatings. *Prog. Org. Coat.* **2018**, *124*, 33–40. [CrossRef]
19. Fombuena, V.; Bernardi, L.; Fenollar, O.; Boronat, T.; Balart, R. Characterization of green composites from biobased epoxy matrices and bio-fillers derived from seashell wastes. *Mater. Des.* **2014**, *57*, 168–174. [CrossRef]
20. Yao, Z.; Xia, M.; Ge, L.; Chen, T.; Li, H.; Ye, Y.; Zheng, H. Mechanical and thermal properties of polypropylene (PP) composites filled with CaCO3 and shell waste derived bio-fillers. *Fibers Polym.* **2014**, *15*, 1278–1287. [CrossRef]
21. Moustafa, H.; Youssef, A.M.; Duquesne, S.; Darwish, N.A. Characterization of bio-filler derived from seashell wastes and its effect on the mechanical, thermal, and flame retardant properties of ABS composites. *Polym. Compos.* **2017**, *38*, 2788–2797. [CrossRef]
22. Wang, F.; Liu, H.; Yan, L.; Feng, Y. Comparative Study of Fire Resistance and Anti-Ageing Properties of Intumescent Fire-Retardant Coatings Reinforced with Conch Shell Bio-Filler. *Polymers* **2021**, *13*, 2620. [CrossRef] [PubMed]
23. Li, Y.; Feng, Y.; Xu, Z.; Yan, L.; Xie, X.; Wang, Z. Synergistic effect of clam shell bio-filler on the fire-resistance and char formation of intumescent fire-retardant coatings. *J. Mater. Res. Technol.* **2020**, *9*, 14718–14728. [CrossRef]
24. Palaniyappan, S.; Veiravan, A.; Kaliyamoorthy, R.; Kumar, V.; Veeman, D. A spatial distribution effect of almond shell bio filler on physical, mechanical, thermal deflection and water absorption properties of vinyl ester polymer composite. *Polym. Compos.* **2022**, *43*, 3204–3218. [CrossRef]
25. Qaiss, A.; Bouhfid, R.; Essabir, H. Characterization and use of coir, almond, apricot, argan, shells, and wood as reinforcement in the polymeric matrix in order to valorize these products. In *Agricultural Biomass Based Potential Materials*; Springer: Berlin/Heidelberg, Germany, 2015; pp. 305–339.
26. Muniyadi, M.; Ng, T.Y.S.; Munusamy, Y.; Ooi, Z.X. Mimusops elengi seed Shell powder as a new bio-filler for polypropylene-based bio-composites. *BioResources* **2018**, *13*, 272–289. [CrossRef]
27. Prabhakar, M.; Shah, A.U.R.; Rao, K.C.; Song, J.-I. Mechanical and thermal properties of epoxy composites reinforced with waste peanut shell powder as a bio-filler. *Fibers Polym.* **2015**, *16*, 1119–1124. [CrossRef]
28. Zuluaga-Parra, J.D.; Ramos-deValle, L.F.; Sánchez-Valdes, S.; Torres-Lubián, J.R.; Rodriguez-Fernadez, O.S.; Hernández-Hernández, E.; da Silva, L.; Rodríguez-Gonzalez, J.A.; Borjas-Ramos, J.J.; Vázquez-Rodríguez, S. Phosphorylated avocado seed: A renewable biomaterial for preparing a flame retardant biofiller. *Fire Mater.* **2022**, *46*, 968–980. [CrossRef]

29. Suthan, R.; Jayakumar, V.; Bharathiraja, G. Wear analysis of bio-fillers reinforced epoxy composites. *Mater. Today Proc.* **2020**, *22*, 793–798. [CrossRef]

30. Gullon, P.; Gullon, B.; Astray, G.; Carpena, M.; Fraga-Corral, M.; Prieto, M.A.; Simal-Gandara, J. Valorization of by-products from olive oil industry and added-value applications for innovative functional foods. *Food Res. Int.* **2020**, *137*, 109683. [CrossRef]

31. Inglezakis, V.; Moreno, J.; Doula, M. Olive oil waste management EU legislation: Current situation and policy recommendations. *Int. J. Chem. Environ. Eng. Syst.* **2012**, *3*, 65–77.

32. Valvez, S.; Maceiras, A.; Santos, P.; Reis, P.N. Olive stones as filler for polymer-based composites: A review. *Materials* **2021**, *14*, 845. [CrossRef]

33. Banat, R. Olive pomace flour as potential organic filler in composite materials: A brief review. *Am. J. Polym. Sci* **2019**, *9*, 10–15.

34. Hernández-Beltrán, J.U.; Hernández-De Lira, I.O.; Cruz-Santos, M.M.; Saucedo-Luevanos, A.; Hernández-Terán, F.; Balagurusamy, N. Insight into pretreatment methods of lignocellulosic biomass to increase biogas yield: Current state, challenges, and opportunities. *Appl. Sci.* **2019**, *9*, 3721. [CrossRef]

35. Hamida, B.; Ahmed, M.; Nadia, N.; Samira, M. Mechanical properties of polystyrene/olive stone flour composites. *Res. J. Pharm. Biol. Chem. Sci.* **2015**, *6*, 127–132.

36. Koutsomitopoulou, A.; Bénézet, J.; Bergeret, A.; Papanicolaou, G. Preparation and characterization of olive pit powder as a filler to PLA-matrix bio-composites. *Powder Technol.* **2014**, *255*, 10–16. [CrossRef]

37. Jozić, S.P.; Jozić, D.; Erceg, M.; Andričić, B.; Bernstorff, S. Nonisothermal crystallization of poly (L-lactide) in poly (L-lactide)/olive stone flour composites. *Thermochim Acta* **2020**, *683*, 178440. [CrossRef]

38. Rodríguez, G.; Lama, A.; Rodríguez, R.; Jiménez, A.; Guillén, R.; Fernández-Bolanos, J. Olive stone an attractive source of bioactive and valuable compounds. *Bioresour. Technol.* **2008**, *99*, 5261–5269. [CrossRef] [PubMed]

39. Reis, P.; Ferreira, J.; Silva, P. Mechanical behaviour of composites filled by agro-waste materials. *Fibers Polym.* **2011**, *12*, 240–246. [CrossRef]

40. Costa, J.; Capela, C.; Ferreira, J. Mechanical behaviour of PVC/CaCO$_3$ particulate composites–influence of temperature. *Strain* **2011**, *47*, 292–304. [CrossRef]

41. Naghmouchi, I.; Mutjé, P.; Boufi, S. Polyvinyl chloride composites filled with olive stone flour: Mechanical, thermal, and water absorption properties. *J. Appl. Polym. Sci.* **2014**, *131*, 41083. [CrossRef]

42. Khalil, A.M.; El-Nemr, K.F.; Hassan, M.L. Acrylate-modified gamma-irradiated olive stones waste as a filler for acrylonitrile butadiene rubber/devulcanized rubber composites. *J. Polym. Res.* **2019**, *26*, 249. [CrossRef]

43. Calovi, M.; Rossi, S. Olive pit powder as multifunctional pigment for waterborne paint: Influence of the bio-based filler on the aesthetics, durability and mechanical features of the polymer matrix. *Ind Crop. Prod* **2023**, *194*, 116326. [CrossRef]

44. Nassar, M.M.; Sider, I. Evaluation of Novel Compatibility Strategies for Improving the Performance of Recycled Low-Density Polyethylene Based Biocomposites. *Polymers* **2021**, *13*, 3486. [CrossRef] [PubMed]

45. Ryu, J.; Ahn, S.; Kim, S.-G.; Kim, T.; Lee, S.J. Interactive ion-mediated sap flow regulation in olive and laurel stems: Physicochemical characteristics of water transport via the pit structure. *PLoS ONE* **2014**, *9*, e98484. [CrossRef] [PubMed]

46. Available online: https://www.bio-powder.com/en/olive-pit/ (accessed on 8 August 2022).

47. Arkles, B. Hydrophobicity, hydrophilicity and silane surface modification. *Gelest. Inc.* **2011**, *215*, 547–1015.

48. Nakamura, T.; Tabuchi, H.; Hirai, T.; Fujii, S.; Nakamura, Y. Effects of silane coupling agent hydrophobicity and loading method on water absorption and mechanical strength of silica particle-filled epoxy resin. *J. Appl. Polym. Sci.* **2020**, *137*, 48615. [CrossRef]

49. Saji, V.S. Wax-based artificial superhydrophobic surfaces and coatings. *Colloids Surf. A Physicochem. Eng. Asp.* **2020**, *602*, 125132. [CrossRef]

50. Xie, Y.; Hill, C.A.; Xiao, Z.; Militz, H.; Mai, C. Silane coupling agents used for natural fiber/polymer composites: A review. *Compos. Part A Appl. Sci.* **2010**, *41*, 806–819. [CrossRef]

51. Available online: https://www.bio-powder.com/en/olive-pit/hydrophobic-olive-stone-functional-powder-h50-h100 (accessed on 15 September 2022).

52. *ASTM B117:2011*; Operating Salt Spray (Fog) Apparatus. ASTM International: West Conshohocken, PA, USA, 2011; pp. 1–12.

53. *ASTM D7334–08*; Standard Practice for Surface Wettability of Coatings, Substrates and Pigments by Advancing Contact Angle Measurement. ASTM International: West Conshohocken, PA, USA, 2008; pp. 1–3.

54. *GB/T 1733-93*; Determination of Resistance to Water of Films. Standardization Administration of the People's Republic of China: Beijing, China, 1993.

55. *ASTM D4587-11(2019)e1*; Standard Practice for Fluorescent UV-Condensation Exposures of Paint and Related Coatings. ASTM International: West Conshohocken, PA, USA, 2019; pp. 1–6.

56. Hassaini, L.; Kaci, M.; Touati, N.; Pillin, I.; Kervoelen, A.; Bruzaud, S. Valorization of olive husk flour as a filler for biocomposites based on poly (3-hydroxybutyrate-co-3-hydroxyvalerate): Effects of silane treatment. *Polym. Test.* **2017**, *59*, 430–440. [CrossRef]

57. Gharbi, A.; Hassen, R.B.; Boufi, S. Composite materials from unsaturated polyester resin and olive nuts residue: The effect of silane treatment. *Ind. Crop. Prod.* **2014**, *62*, 491–498. [CrossRef]

58. Naghmouchi, I.; Mutjé, P.; Boufi, S. Olive stones flour as reinforcement in polypropylene composites: A step forward in the valorization of the solid waste from the olive oil industry. *Ind. Crop. Prod.* **2015**, *72*, 183–191. [CrossRef]

59. Tserki, V.; Matzinos, P.; Kokkou, S.; Panayiotou, C. Novel biodegradable composites based on treated lignocellulosic waste flour as filler. Part I. Surface chemical modification and characterization of waste flour. *Compos. Part A Appl. Sci.* **2005**, *36*, 965–974. [CrossRef]

60. Calovi, M.; Rossi, S.; Deflorian, F.; Dirè, S.; Ceccato, R. Graphene-based reinforcing filler for double-layer acrylic coatings. *Materials* **2020**, *13*, 4499. [CrossRef] [PubMed]
61. *ASTM E308-18*; Standard Practice for Computing the Colors of Objectives by Using the CIE System. ASTM International: West Conshohocken, PA, USA, 2018; pp. 1–45.
62. Calovi, M.; Rossi, S. Durability of Acrylic Cataphoretic Coatings Additivated with Colloidal Silver. *Coatings* **2022**, *12*, 486. [CrossRef]
63. Hasani, M.; Mahdavian, M.; Yari, H.; Ramezanzadeh, B. Versatile protection of exterior coatings by the aid of graphene oxide nano-sheets; comparison with conventional UV absorbers. *Prog. Org. Coat.* **2018**, *116*, 90–101. [CrossRef]
64. *ISO 4628*; Evaluation of Degradation of Coatings. ISO: Geneva, Switzerland, 2012.
65. Gašparovič, L.; Koreňová, Z.; Jelemenský, Ľ. Kinetic study of wood chips decomposition by TGA. *Chem. Pap.* **2010**, *64*, 174–181. [CrossRef]
66. Yang, H.-S.; Kim, H.-J.; Park, H.-J.; Lee, B.-J.; Hwang, T.-S. Water absorption behavior and mechanical properties of lignocellulosic filler–polyolefin bio-composites. *Compos. Struct.* **2006**, *72*, 429–437. [CrossRef]
67. Yan, X.; Wang, L.; Qian, X. Influence of thermochromic pigment powder on properties of waterborne primer film for Chinese fir. *Coatings* **2019**, *9*, 742. [CrossRef]
68. Yan, X.; Wang, L.; Qian, X. Effect of coating process on performance of reversible thermochromic waterborne coatings for Chinese Fir. *Coatings* **2020**, *10*, 223. [CrossRef]
69. Yan, X.; Qian, X.; Chang, Y.; Lu, R.; Miyakoshi, T. The effect of glass fiber powder on the properties of waterborne coatings with thermochromic ink on a Chinese Fir surface. *Polymers* **2019**, *11*, 1733. [CrossRef]
70. *GB/T 11186.3-1989*; Method of Measurement of Coating Color. Part III: Calculation of Chromatic Aberration. SAC: Beijing, China, 1990.
71. Yousif, E.; Haddad, R. Photodegradation and photostabilization of polymers, especially polystyrene. *SpringerPlus* **2013**, *2*, 398. [CrossRef]
72. Zhang, T.; Wu, W.; Wang, X.; Mu, Y. Effect of average functionality on properties of UV-curable waterborne polyurethane-acrylate. *Prog. Org. Coat.* **2010**, *68*, 201–207. [CrossRef]
73. Decker, C.; Masson, F.; Schwalm, R. Weathering resistance of waterbased UV-cured polyurethane-acrylate coatings. *Polym. Degrad. Stab.* **2004**, *83*, 309–320. [CrossRef]
74. Ishigaki, T.; Sugano, W.; Ike, M.; Taniguchi, H.; Goto, T.; Fujita, M. Effect of UV irradiation on enzymatic degradation of cellulose acetate. *Polym. Degrad. Stab.* **2002**, *78*, 505–510. [CrossRef]
75. Cogulet, A.; Blanchet, P.; Landry, V. Wood degradation under UV irradiation: A lignin characterization. *J. Photochem. Photobiol. B Biol.* **2016**, *158*, 184–191. [CrossRef] [PubMed]
76. Kunwong, D.; Sumanochitraporn, N.; Kaewpirom, S. Curing behavior of a UV-curable coating based on urethane acrylate oligomer: The influence of reactive monomers. *Songklanakarin J. Sci. Technol.* **2011**, *33*, 201.
77. Bahadur, A.; Shoaib, M.; Saeed, A.; Iqbal, S. FT-IR spectroscopic and thermal study of waterborne polyurethane-acrylate leather coatings using tartaric acid as an ionomer. *e-Polymers* **2016**, *16*, 463–474. [CrossRef]
78. Mashouf, G.; Ebrahimi, M.; Bastani, S. UV curable urethane acrylate coatings formulation: Experimental design approach. *Pigment. Resin Technol.* **2014**, *43*, 61–68. [CrossRef]
79. Fengel, D.; Wegener, G. *Wood: Chemistry, Ultrastructure, Reactions*; Walter de Gruyter: Berlin, Germany, 2011.
80. Ghavidel, A.; Bak, M.; Hofmann, T.; Vasilache, V.; Sandu, I. Evaluation of some wood-water relations and chemometric characteristics of recent oak and archaeological oak wood (Quercus Robur) with archaeometric value. *J. Cult. Herit.* **2021**, *51*, 21–28. [CrossRef]
81. Ghavidel, A.; Hosseinpourpia, R.; Gelbrich, J.; Bak, M.; Sandu, I. Microstructural and chemical characteristics of archaeological white elm (*Ulmus laevis* P.) and poplar (*Populus* spp.). *Appl. Sci.* **2021**, *11*, 10271. [CrossRef]
82. Gu, Y.; Bian, H.; Wei, L.; Wang, R. Enhancement of hydrotropic fractionation of poplar wood using autohydrolysis and disk refining pretreatment: Morphology and overall chemical characterization. *Polymers* **2019**, *11*, 685. [CrossRef]
83. Calovi, M.; Coroneo, V.; Palanti, S.; Rossi, S. Colloidal silver as innovative multifunctional pigment: The effect of Ag concentration on the durability and biocidal activity of wood paints. *Prog. Org. Coat.* **2023**, *175*, 107354. [CrossRef]
84. Deflorian, F.; Rossi, S. An EIS study of ion diffusion through organic coatings. *Electrochim. Acta* **2006**, *51*, 1736–1744. [CrossRef]
85. Akbarinezhad, E.; Bahremandi, M.; Faridi, H.; Rezaei, F. Another approach for ranking and evaluating organic paint coatings via electrochemical impedance spectroscopy. *Corros. Sci.* **2009**, *51*, 356–363. [CrossRef]
86. Macdonald, J.R.; Barsoukov, E. *Impedance Spectroscopy: Theory, Experiment, and Applications*; John Wiley & Sons: Hoboken, NJ, USA, 2018.
87. Calovi, M.; Russo, F.; Rossi, S. Synergic behavior of graphene-based filler and thermochromic pigments in cataphoretic coatings. *Prog. Org. Coat.* **2021**, *150*, 105978. [CrossRef]